WILEY-VCH

Methanol synthesis at a wide range of H_2/CO_2 ratios over Rh-In bimetallic catalyst

Molly Meng-Jung Li[†], Hanbo Zou[†], Jianwei Zheng[†], Tai-Sing Wu, Ting-Shan Chan, Yun-Liang Soo, Xin-Ping Wu, Xue-Qing Gong, Tianyi Chen, Kanak Roy, Georg Held, Shik Chi Edman Tsang*

Abstract: Recent years have seen an increasing interest in capturing hydrogen generated from renewables with CO_2 to produce methanol. However, renewable hydrogen production is currently expensive and in limited quantity as compared to CO_2. Excess CO_2 and limited H_2 in the feedstock gas mixture is not favourable for the CO_2 hydrogenation to methanol reaction, which causes low activity and poor methanol selectivity. Here we report a new class of Rh-In catalysts with optimal adsorption property to the intermediates of methanol production. The Rh-In catalyst can effectively catalyse methanol synthesis but inhibit reverse water-gas shift reaction under H_2-deficient gas flow and shows the best competitive methanol productivity under industrially applicable conditions in comparison with the literature reported values. This work demonstrates a strong potential of Rh-In bimetallic composition, from which a convenient methanol synthesis based on flexible feedstock compositions (e.g. H_2/CO_2 from biomass derivatives) with lower energy cost can be established.

Table of Contents

SUPPORTING INFORMATION

1. Supplementary experimental information

1.1 Synthesis of the indium-aluminum oxides support

The binary metal oxide supports were synthesised using a co-precipitation method. The metal precursors were hydrated metal nitrate salts: $Al(NO_3)_2 \cdot 3H_2O$ (Aldrich) and $In(NO_3)_3 \cdot xH_2O$ (Aldrich). Indium and aluminium metal nitrates with a desired In/Al ratio were dissolved completely in 150 mL deionised water to make a solution with a concentration of 0.05M. A Na_2CO_3 aqueous solution was prepared by dissolving 7.5 g of Na_2CO_3 in 300 mL of deionised water. The solutions were added simultaneously into a beaker containing 50 mL of preheated deionised water at 80 °C. A delivery pump was used to inject the metal nitrate solution at a constant rate of 0.4 mL min^{-1} in an automatic and reproducible manner. An HPLC pump was used to deliver the Na_2CO_3 solution at a rate of 0.4-0.8 mL min^{-1}. The mixture was stirred at 1,000 rpm, with the pH of the precipitating solution carefully maintained at 9 ± 0.1. Once the addition of the precursor metal nitrate solution was completed, the resulting precipitate was aged in the solution for 18 h. After the aging process, the precipitate was extracted by centrifugation at 5,000 rpm. The centrifuged precipitate was washed with deionised water several times at 5,000 rpm to remove residual Na^+ ions and then washed with acetone before drying in a vacuum. The dried powder was then calcined in N_2 at a ramp of 5 °C min^{-1} up to the desired temperature (450 °C, if not indicated) for 4 h to get the final indium and aluminum oxide supports.

1.2 Synthesis of the indium-modified Rh, indium-modified Ru samples with different In/Al ratios.

The detailed information of the samples is listed in Table 1 of the main manuscript. In this part, the samples are classified into two categories: Those loaded Rh or Ru by the wet-impregnation method and those by co-precipitation method. For the wet-impregnation samples: Rhodium-indium supports with different recipe In:Al ratios were firstly synthesised using co-precipitation method. Then the derived support was immersed into an $Rh(NO_3)_3$ (Aldrich) aqueous solution and the mixture was kept stirring until the solid and liquid were mixed evenly. The slurry was set aside in air for one night before drying in an oven at 80 °C. The dried powder was then calcined in N_2 at a ramp of 5 °C min^{-1} up to 450 °C for 4 h to get the final binary metal oxides supported Rh samples. The co-precipitation samples were prepared by the following process: metal nitrates ($Rh(NO_3)_3$ aqueous solution, $Al(NO_3)_2 \cdot 3H_2O$ and/or $In(NO_3)_3 \cdot xH_2O$) were dissolved completely in 150 mL deionised water to make a solution with a concentration of 0.05M. A Na_2CO_3 aqueous solution was prepared by dissolving 7.5 g of Na_2CO_3 in 300 mL of deionised water. The solutions were added simultaneously into a plastic reactor containing 50 mL of preheated deionised water at 80 °C. A delivery pump was used to inject the metal nitrate solution at a constant rate of 0.4 mL min^{-1} in an automatic and reproducible manner. An HPLC pump was used to deliver the Na_2CO_3 solution at a rate of 0.4-0.8 mL min^{-1}. The mixture was stirred at 1,000 rpm, with the pH of the precipitating solution carefully maintained at 9 ± 0.1. Once the addition of the precursor metal nitrate solution was completed, the resulting precipitate was aged in the solution for 18 h. After the aging process, the precipitate was extracted by centrifugation at 5,000 rpm. The centrifuged precipitate was washed with deionised water several times at 5,000 rpm to remove residual Na^+ ions and then washed with acetone before drying in a vacuum. The dried powder was then calcined in N_2 at a ramp of 5 °C min^{-1} up to the desired temperature (450 °C, if not indicated) for 4 h to get the final catalysts.

1.3 Catalytic testing of CO_2 hydrogenation reaction

Catalytic testing in hydrogenation of CO_2 to produce methanol was carried out in a tubular fixed-bed reactor (12.7 mm outside diameter) by using a catalyst weight of 0.1 g. Commercial $Cu/ZnO/Al_2O_3$ catalyst (HiFUEL R120, Johnson Matthey) was used as the benchmark catalyst for the catalyst comparison. Before each test, the catalyst was pre-reduced at 290 °C for 2 h under the H_2 flow of 20 STP mL min^{-1} (STP = standard temperature and pressure; P = 101.3 kPa, T = 298 K). Once the reduction was completed, the catalyst bed was then cooled down to room temperature. CO_2/H_2 reaction mixture with molar ratios ranging from $CO_2 : H_2$ = 1 : 3 to 3 : 1 were fed into the reactor at a constant rate (depending on the WHSV applied, for WHSV = 18000 mL g^{-1} h^{-1} the flow rate is 30mL min^{-1}) through the catalyst bed, and the system pressure was held at the desired pressure (1 bar, 20bar, or 45bar) controlled by a back-pressure regulator. After the pressure reached the target pressure and stabilised,

the reactant mixture composition was analysed by an online gas chromatograph equipped with two thermal conductivity detectors (TCD) and one flame ionisation detector (FID) with methanizer to get the peak areas of the unreacted CO_2 and H_2 for the calculations of the conversions. Afterwards, the system temperature was increased to 210 °C at a heating rate of 10 °C min^{-1}. After the stabilisation period of 2 hours, during which the temperature and pressure were both stabilised, the catalytic activity was repeatedly measured for 2 hours through monitoring the outlet gas composition by the online gas chromatograph and stable CO_2 conversions were detected (the typical standard deviations lower than 0.1%). The reaction temperature was then increased to 230 °C, 250 °C, 270 °C, 290 °C, 310 °C and the same catalytic activity recording procedure was applied on each temperature condition. The methanol space time yield (STY), expressed as gram of methanol per hour and per gram of catalyst, was calculated using the methanol production rate (methanol concentration in the outlet gas from the reactor per unit time) and the weight of the catalyst in the calcined form (0.1g) without considering oxygen loss during reduction.

Notice that we performed most of the catalytic testing under the condition of H_2/CO_2 ratio = 3 in a fair comparative manner.

1.4 Characterisation Techniques

X-ray powder diffraction (XRD)
The X-ray diffraction (XRD) profile was collected by a Philips PW-1729 diffractometer with Bragg-Brentano focusing geometry using Cu Ka radiation (lambda= 1.5418 Å) from a generator operating at 40 kV and 40 mA.

X-ray photoelectron spectroscopy (XPS)
After the reduction in H_2 at 290 °C, the reduced samples were carefully transferred in a glove bag filled with N_2 to prevent air exposure and analysed by XPS. XPS was performed using a Quantum 2000 Scanning ESCA Microprobe instrument (Physical Electronics) equipped with an Al Kα X-ray radiation source (hv = 1486.6 eV). A flood gun with variable electron voltage (from 6 eV to 8 eV) was used for charge compensation. The raw data were corrected for substrate charging with the BE of the C peak at 285 eV, as shown in the XPS handbook. The measured spectra were fitted using a least-squares procedure to a product of Gaussian–Lorentzian functions after removing the background noise. The concentration of each element was calculated from the area of the corresponding peak and calibrated with the sensitivity factor of Wagner.

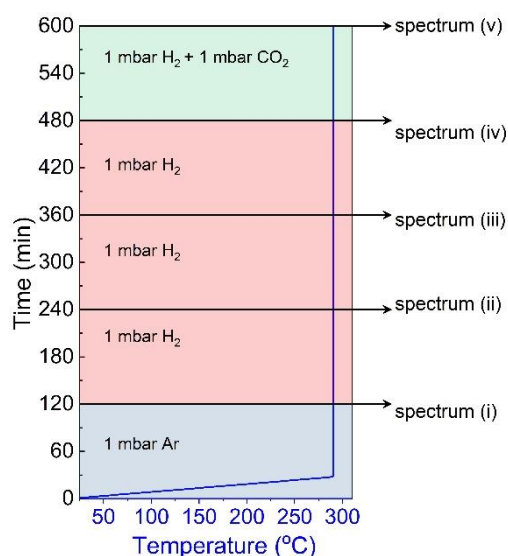Near ambient-pressure X-ray photoelectron spectroscopy (NAP-XPS)
APXPS measurements were carried out at Versatile Soft X-ray (VERSOX) beamline B07 of Diamond Light Source. VERSOX is a soft x-ray (energy range 50-2800 eV) bending magnet beamline fitted with a differentially pumped nozzle that allows successful operation up to 100 mbar in the endstation without using any membrane. The beamline endstation, equipped with a differentially pumped Specs Phoibos 150 NAP electron analyzer, allows in situ measurements of solid samples while dosing a gas/gas mixture in mbar range. In the geometry adopted during the experiments, photoelectrons were detected at an angle of 54.7° with respect to the direction of the surface normal, and linearly polarized light was used throughout the experiments.

3mg of the calcined co-RhIn/(5In5Al)O powder was dispersed in 5mL ethanol followed by drop-casting and drying (at room temperature) to form a thin film on a gold-coated silicon wafer with an area of ca. 0.5 cm^2. The wafer was mounted onto a sample holder. The sample was heated in resistive mode, and the temperature was monitored with a K type (Ni/NiCr) thermocouple attached to the sample. Ultrapure gases were introduced through precise leak valves. The experiments were performed under following conditions: (i) the sample was exposed to 1 mbar Ar and heated to 290 °C for around 120 mins, (ii) chamber was vacuumed to lower than 0.0001 mbar and the gas feed was switched from Ar to H_2 to reach 1 mbar for 120 mins (1st H_2 exposure), (iii) the catalyst was exposed to 1 mbar H_2 and held for 120 mins (2nd H_2 exposure), (iv) the catalyst was exposed to 1 mbar H_2 and held for 120 mins (3rd H_2 exposure), (v) chamber was vacuumed to lower than 0.0001 mbar and then the catalyst was exposed

to 1 mbar H_2 + 1 mbar CO_2 and held for 120 mins. The experiment steps (i) to (v) are sketched in the figure below.

Core level photoemission spectra were recorded at a constant temperature at 290 °C in each condition listed above (i~v). *Rh* 3d and *In* 3d spectral regions were recorded using the incident photon energy of 1210 and 1340 eV, respectively, to ensure a similar probed depth. The spectra were corrected using the Fermi edge position. After subtraction of a Shirley background, the photoemission peaks were deconvoluted using Gaussian functions.

Fig. S1. The scheme of the NAP-XPS experiment procedures

X-ray absorption spectroscopy (XAS) Rh K-edge & Rh, In L-edge
After the reduction in H_2 at 290 °C, the reduced samples were carefully transferred to a nitrogen glove box. The reduced samples were then sandwiched and dispersed between Scotch Tape for the XAS experiments. Local structures surrounding Rh atoms were probed by using XAS technique at beamline BL01C of Taiwan Light Source at the National Synchrotron Radiation Research Center (NSRRC) in Taiwan. A Si(111) Double Crystal Monochromator (DCM) was used to scan the photon energy. The energy resolution ($\Delta E/E$) for the incident X-ray photons was estimated to be 2×10^{-4}. Fluorescence mode was adopted for Rh K-edge XAS measurements. To ascertain the reproducibility of the experimental data, at least two scan sets were collected and compared for each sample. The Rh and In L_3-edge X-ray absorption near edge structure (XANES) spectra were recorded with a beamline 16A1. The EXAFS data analysis was performed using Athena and Artemis. The spectra were calibrated with Rh foils as a reference to avoid energy shifts of the samples, and the amplitude reducing factor was obtained from EXAFS data analysis of the foil, which was used as a fixed input parameter in the data fitting to allow the refinement in the coordination number of the absorbing atom. In this work, the first shell data analyses under the assumption of single scattering were performed with the errors estimated by R-factor.

Temperature-programmed reduction (TPR)
Temperature-programmed reduction (TPR) measurements were obtained using a ThermoQuest TPRO 1100 instrument. Inside the TPR quartz tube, 0.02 g of the calcined catalyst sample was sandwiched between glass wool, and a thermocouple was placed in contact with the sample during the measurement. The TPR tube was placed into the instrument for a helium pretreatment. The helium gas pretreatment (He running through the TPR tube at 10 mL min⁻¹ at a temperature ramp of 10 °C min⁻¹ from 40 to 150 °C, then held for 5 min before cooling) was employed to clean the catalyst surface by removing any absorbed ambient gas molecules. After the He pretreatment, a reduction treatment (5% H_2 in Argon flowing through the TPR tube at 20 mL min⁻¹ at a temperature ramp of 10 °C min⁻¹ from 40 to 600 °C then cooling to room temperature) was carried out to reduce the Rh species and the surface In species in the sample.

The consumption of hydrogen gas changed the conductivity of the gas stream; therefore, the change in conductivity was measured and calibrated as a function of both temperature and time to produce the H_2-TPR profile.

Transmission electron microscopy (TEM)

Transmission electron microscopy (TEM) images were taken using an aberration-corrected TEM JEOL 2200MCO operated at 80kV. Samples were reduced in H_2 at 290 °C then dispersed in 1 mL ethanol for 15 minutes (in N_2 atmosphere) before the dropwise addition of the solution onto Agar Scientific Holey carbon-supported copper 400 mesh grid. After drying the samples were quickly placed into the vacuum chamber of the TEM to prevent or minimise re-oxidation.

In-situ Fourier transform infrared spectroscopy (FTIR)

In situ Fourier transform infrared (*in-situ* FTIR) spectra were recorded using a Thermo Scientific Nicolet 6700 FTIR spectrometer equipped with a Specac's high-temperature high-pressure cell. Spectra were obtained by collecting 32 scans with a resolution of 4 cm^{-1} and are presented in absorbance units. The powders of the co-Rh/Al_2O_3 sample, co-RhIn/(5In5Al)O sample and the commercial Cu/ZnO/Al_2O_3 catalyst were pressed into pellets and loaded onto the sample holder. The sample was then flushed with 5% H_2/Ar (20 mL min^{-1}) for 20 min and then reduced for 2 h at 290 °C. After the pre-reduction, the backgrounds were recorded at 50 °C, 100 °C, 150 °C, 200 °C, 250 °C and 290 °C in the atmosphere of 5% H_2/Ar. After collecting the backgrounds, a gas mixture of CO_2/H_2 = 1/3 was passed through the reduced sample pellet and then the in situ FTIR spectra were collected at 50 °C, 100 °C, 150 °C, 200 °C, 250 °C and 290 °C with each temperature maintained for at least 30 min.

BET surface area analysis

The surface area of the samples was determined by N_2 adsorption-desorption at a liquid nitrogen temperature of -196 °C using the Micromeritics ASAP 2020M Analyzer. Sample degassing was carried out at 200 °C for 3 h prior to the acquisition of the adsorption isotherm. Calculations were conducted according to the Brunauer–Emmett–Teller (BET) method.

Hydrogen/Oxygen titration method for measurement of Rh dispersion

The metal dispersion analysis was conducted on the PCA-1200 Chemisorption Analyzer (Bejing Biaode Electronic Technology Co., Ltd, China). The samples were degassed at 300 °C for 1 hour under a constant helium flow (30 mL min^{-1}). After that, the samples were reduced in hydrogen (30 mL min^{-1}) at 400 °C for 1 hour. After cooling down to 100 °C in helium, the samples were then oxidised with oxygen (20 mL min^{-1}) at for 1h. The oxidised samples were then reduced at 200 °C with pulsed hydrogen until the peak area of hydrogen recorded by a thermal conductivity detector was unchanged. The metal dispersion was calculated based on the consumption of hydrogen.

Thermodynamic predictions of equilibrium reaction states

To get the reaction states according to equilibrium thermodynamics of the CO_2 hydrogenation to methanol under our reaction conditions, thermodynamics predictions were thus performed to derive the equilibrium thermodynamics values (HSC Chemistry 6) where only the intrinsic properties of the gas species were considered. Here the reactant mixtures of 1 mole of CO_2(g) and 3 moles of H_2(g) were considered, and product species of H_2O(g), CO(g) and CH_3OH(g) (experimentally identified) were taken into account in the calculations.
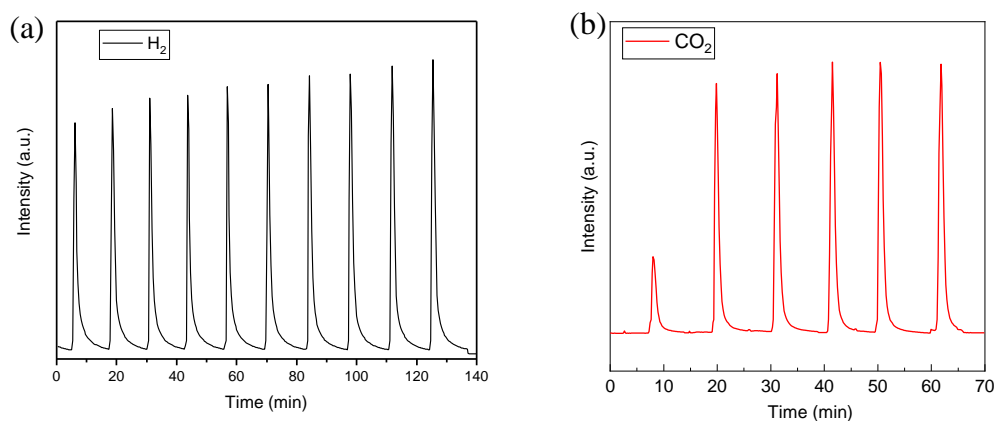
CO_2 and H_2 pulse analysis

Pulse technique is used in this work to determine the surface adsorption under the atmosphere of CO_2 and H_2 mixture over Cu nanoparticles, commercial Cu/ZnO/Al_2O_3, In_2O_3-Al_2O_3 support, co-Rh/Al_2O_3, and co-RhIn/(5In5Al)O samples. To perform the pulse experiment, 500 mg powder was loaded in a quartz micro-reactor of TPDRO 1100 (ThermoQuest). The sample was reduced in H_2 flow at a rate of 20 mL min^{-1} at 330 °C for 2 h. After that, the sample was further heated to 380 °C under an argon flow at a rate of 20 mL min^{-1} for 0.5 h, and then the sample was cooled down to 50 °C for the in-situ chemisorption measurement: A gas mixture (25% CO_2 and 75% H_2) was pulsed through the sample 10 times via a high precision 0.445 mL loop valve system. The gas composition at the outlet of the micro-reactor was

analysed by an online mass spectrometer. An example of mass spectroscopic peaks for H_2 (m/z = 2) over Cu/ZnO/Al$_2$O$_3$ sample is shown in the following figure:

Fig. S2. a) Mass spectroscopic peaks for H_2 (m/z = 2) over Cu/ZnO/Al$_2$O$_3$ sample in the CO$_2$/H$_2$ pulse experiment at 50 °C. b) Mass spectroscopic peaks for CO_2 (m/z = 44) over In$_2$O$_3$/Al$_2$O$_3$ sample in the CO$_2$/H$_2$ pulse experiment at 50 °C

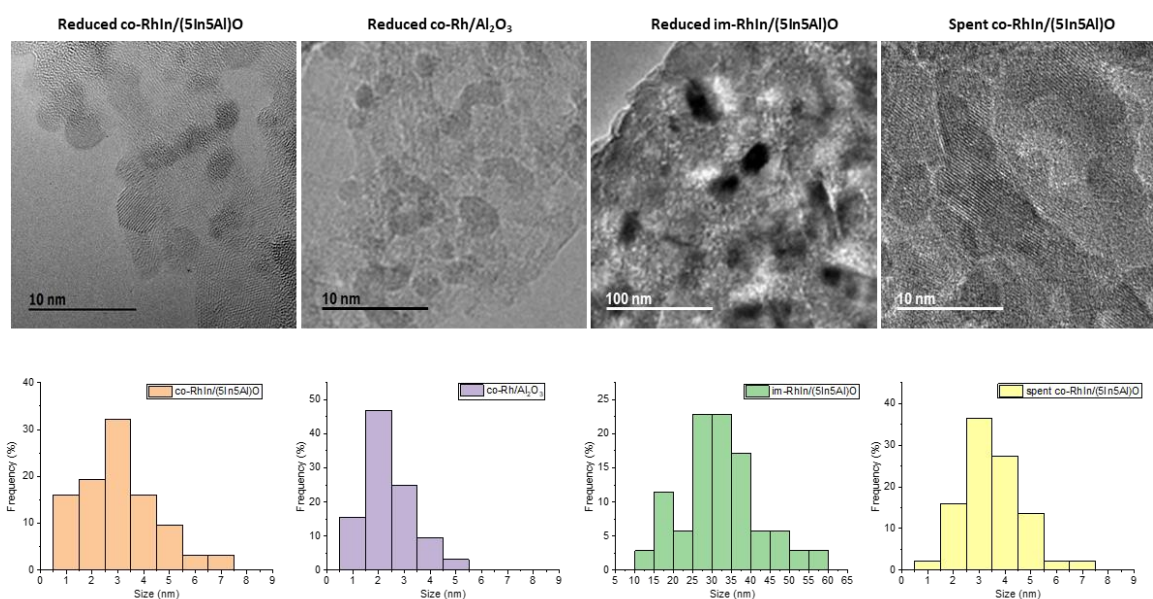The adsorbed CO_2 or H_2 amounts were then calculated based on the following equation,

$$D = \frac{N}{m * A} * \sum_{1}^{n=7} (A - A1) + (A - A2) + \cdots + (A - An)$$

Where D is the mole number of the adsorbed CO_2 or H_2. N is the mole number of CO_2 or H_2 in each pulse, m is the catalyst amount, A is the averaged area of the last three pulses.
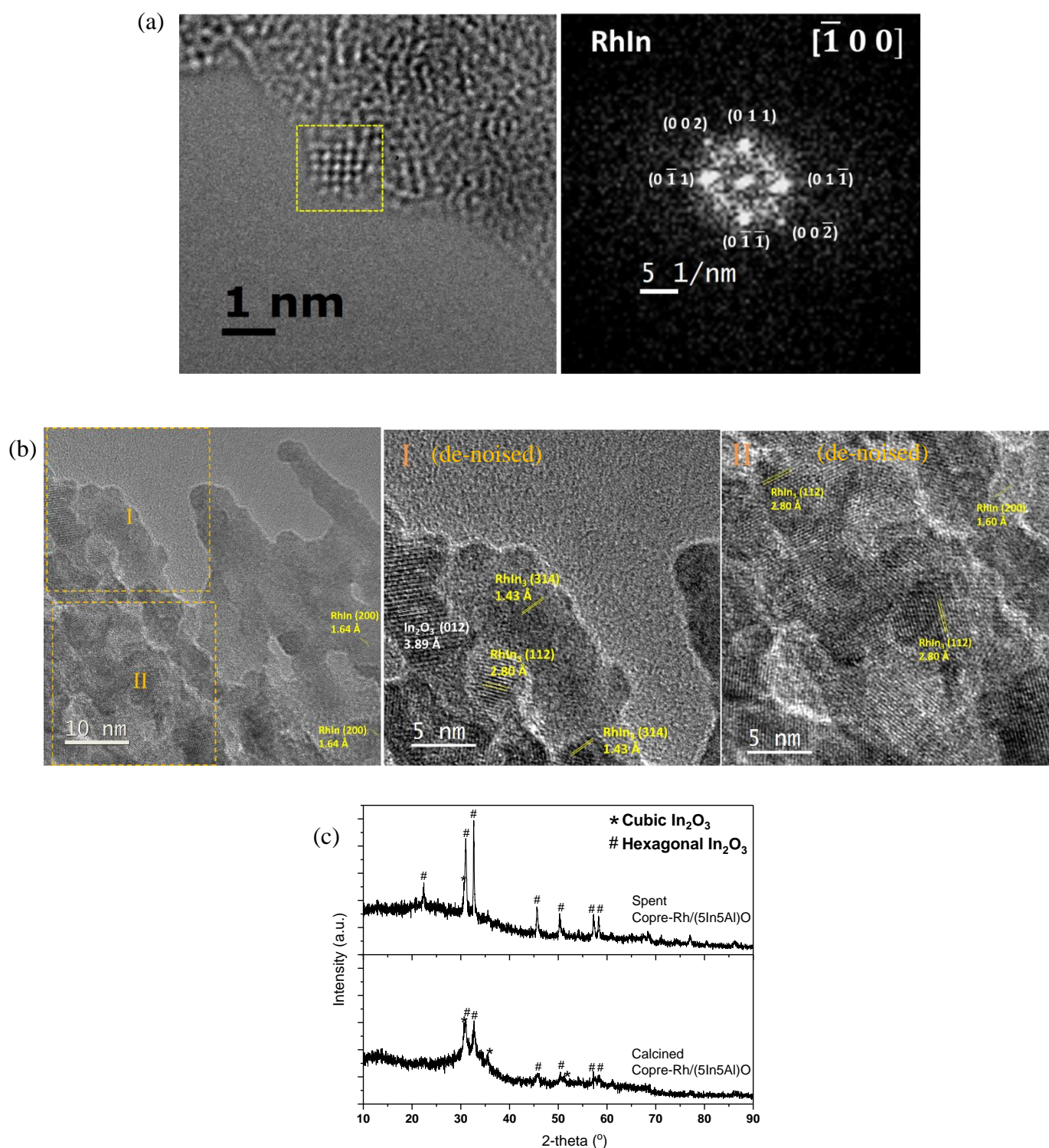
2. Supplementary structural information of the Rh-containing catalysts

Fig. S3. TEM images and particle size distribution diagrams of co-RhIn/(5In5Al)O, co-Rh/Al$_2$O$_3$, im-RhIn/(5In5Al)O treated in H$_2$ atmosphere at 290 °C for 3h, and the spent co-RhIn/(5In5Al)O is the sample retrieved after 24 h TOS test of CO$_2$ hydrogenation at 270 °C, 45bar, CO$_2$/H$_2$=1/3 WHSV = 18000 mL g^{-1} h^{-1}.
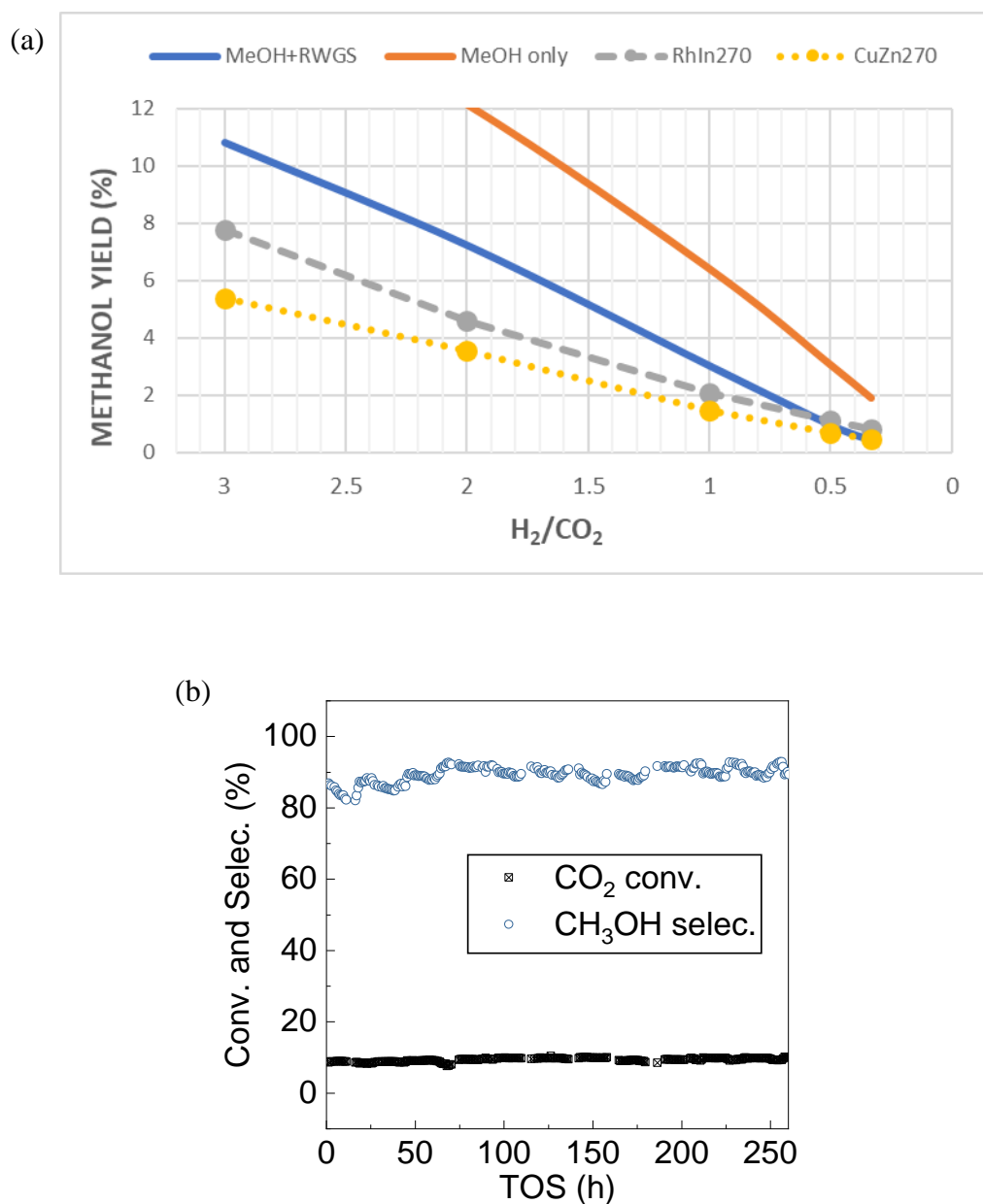
Fig. S4 a) HR-TEM images with the fast-Fourier Transform (FFT) analyses of the selected RhIn alloy nanoparticle in the freshly reduced co-RhIn/(5In5Al)O catalyst. b) HR-TEM images with measured d-spacings corresponding to both the Rh-In alloy nanoparticles and the hexagonal In_2O_3 support in the spent co-RhIn/(5In5Al)O catalyst. Nonlinear filtering was applied in areas I and II to improve the signal-to-noise ratio (see the images captioned "de-noised"). c) XRD patterns of the calcined (in N_2) and spent co-RhIn/(5In5Al)O catalysts.

3. Supplementary catalytic testing results of the In-modified Rh catalyst

Fig. S5. a) Comparison of methanol yields as a function of H_2/CO_2 ratio from co-RhIn/(5In5Al)O and Cu/ZnO/Al$_2$O$_3$ (temperature at 270 °C, pressure at 45 bar) and the maximum achievable methanol yields calculated from thermodynamic equilibrium product compositions. Calculations of thermodynamic equilibrium were performed on HSC Chemistry 6 Software. MeOH+RWGS: considering both methanol synthesis and RWGS routes; MeOH: considering methanol formation only. b) The stability test of CO_2 hydrogenation over co-RhIn/(5In5Al)O at 270 °C, 45bar, CO_2/H_2=1/3 WHSV = 18000 mL g^{-1} h^{-1}. TOS: Time-on-stream.

4. Comparison of Rh-In catalyst to the traditional Cu-based catalysts and the state-of-the-art catalysts

Table S1 gives a list of the state-of-the-art methanol production catalysts compared to the In-modified Rh catalyst in the current study. Note that this table only lists the references that have provided comprehensive catalytic testing data, e.g. CO_2 conversion, methanol selectivity, methanol space-time yield, etc, otherwise references will be discussed and compared in the following text.

In the main paper, we have demonstrated that co-RhIn/(5In5Al)O is superior to the commercial $Cu/ZnO/Al_2O_3$ catalyst (HiFUEL R120, Alfa Aesar) under realistic industrial applicable flow conditions with an acceptable range of H_2/CO_2 ratios (≤ 3). In Table S1 we further disclose that methanol productivity of co-RhIn/(5In5Al)O outperforms the ultrathin LDH-derived CuZnGa catalyst, a catalyst developed by our group that shows the best-reported methanol yield among all the Cu-based catalyst in the literature (catalyst No. 2 in Table S1).[1] The STY of co-RhIn/(5In5Al)O is 17% higher than that of the LDH-derived CuZnGa catalyst under the comparable CO_2 hydrogenation condition. Bimetallic Pd-Zn system[2–4] (see catalysts No. 3&4 in Table S1) is reported to be promising for CO_2 hydrogenation to methanol due to its high selectivity (around 55% to 65%) toward methanol production. However, co-RhIn/(5In5Al)O gives even better methanol selectivity (70% to 90%) under both low-pressure (20 bar) and high-pressure (45 bar) reaction conditions, when compared to those reported Pd-Zn catalyst systems[2–4].

It is noted that for the hydrogenation of CO_2, catalytic performance is highly dependent on the H_2/CO_2 ratio used. Using higher H_2/CO_2 the yield and selectivity to methanol can be enhanced (see Fig. 1 in the main paper). As a result, there have been catalyst screening in the literature using artificial conditions with H_2/CO_2 ratios greater than >>3 to boost the catalytic performance whereas much lower H_2/CO_2 is practically expected. Recently, $Pd-In_2O_3$ catalyst system (catalysts No. 5~7 in Table S1) demonstrates promising methanol productivity,[5–7] but it should be noted that the high methanol STY of 0.89 and 1.01 $g_{MeOH}·g_{cat}^{-1}·h^{-1}$ from Pd/In_2O_3 and $Pd-In_2O_3$ CP catalysts, respectively, were obtained under an H_2-rich condition with $H_2/CO_2 = 4$, temperature of 300 °C, and a high pressure of 50 bar[6,7]. Similarly, the $Cu/CeO_x/TiO_2(100)$ flat model catalyst system provides the combination of metal and oxide sites in the copper-ceria interface, which shows extremely high TOF on methanol synthesis through a distinctive reaction pathway ($CO_2→CO→CH_3OH$).[8] The rate of methanol production on $Cu/CeO_x/TiO_2(110)$ was found to be ~1280 times faster than on Cu(111) and ~87 times faster than on $Cu/ZnO(000\bar{1})$. However, such promising activity was achieved in the extremely high $H_2/CO_2 = 9$, this means that when applying the conditions of $H_2/CO_2 < 3$, the methanol production rate of the $Cu/CeO_x/TiO_2(110)$ surface is expected to drop significantly. Besides, the authors also disclosed a result that the rate of RWGS is much higher than the rate of methanol synthesis: Rates of RWGS and methanol synthesis are estimated to be $1800×10^{15}$ molecules $cm^{-2} s^{-1}$ and $2×10^{15}$ molecules $cm^{-2} s^{-1}$, respectively, at a reaction temperature of 302 °C[8]. This indicates a significantly low methanol selectivity (value was not given by the authors) on the $Cu/CeO_x/TiO_2(110)$ surface. Indeed, similar catalyst systems, e.g., $CeO_x/TiO_2(110)$ supported metal nanoparticles[9] and Cu/CeO_2 powder/nanocatalysts,[9–11] have been demonstrated to be highly active for the (R)WGS reactions. Therefore, to enhance the methanol selectivity and methanol production on the Cu/ceria catalyst system, very high reaction pressure and a reactant gas mixture with a high H_2/CO_2 ratio are therefore required.

Intermetallic compounds of Ni-Ga and Pd-Ga as catalysts[12,13] were reported to have the same or better methanol synthesis rate as well as considerably lower production of CO in comparison with conventional $Cu/ZnO/Al_2O_3$ catalysts under atmospheric reaction pressure. Under such low pressure, our co-RhIn/(5In5Al)O catalyst shows 2 times higher in methanol STY than Ni_5Ga_3/SiO_2 catalyst (catalyst No. 8 in Table S1). Note that under atmospheric pressure, the CO_2 conversion is very low and that results in the difficulties in the actual gas analysis, hence a higher experimental error might be involved. Apart from the above-mentioned active metal-based catalysts, some recent progress has also been found on the metal-oxide based catalysts. Martin et al.[14] reported a highly active and methanol selective $In_2O_3-ZrO_2$ catalyst (catalyst No. 9 in Table S1) with remarkable stability. Compare to our Rh-In system, the $In_2O_3-ZrO_2$ catalyst gave lower CO_2 conversion (5%) hence resulting in lower methanol yield (STY value is less

than half of that from co-RhIn/(5In5Al)O). In another recent study, Wang *et al.*[15] reported a highly active and methanol selective $ZnO-ZrO_2$ solid solution catalyst (catalyst No. 10 in Table S1). Our co-RhIn/(5In5Al)O shows comparable CO_2 conversion, methanol selectivity and methanol yield under the reaction pressure around 45-50 bar. At low reaction pressure (20 bar), our co-RhIn/(5In5Al)O retains a decent CO_2 conversion and methanol productivity (8% CO_2 conversion, 0.36 $g_{MeOH} \cdot g_{cat}^{-1} \cdot h^{-1}$ STY) over the $ZnO-ZrO_2$ catalyst (3.4 % CO_2 conversion, 0.25 $g_{MeOH} \cdot g_{cat}^{-1} \cdot h^{-1}$ STY). This can particularly highlight the advantages of efficient H_2 activation when using the active Rh-In catalyst for the mild reaction conditions.

Overall, our In-modified Rh catalyst has very competitive methanol productivity when in comparison with the literature reported values. Most importantly, the Rh-In catalyst system further displays its advantages in terms of effective methanol production under H_2-deficient/low H_2 coverage conditions and efficient H_2 utilisation while minimising RWGS reaction.

SUPPORTING INFORMATION

Table S1 Comparison of indium-modified rhodium catalyst to the traditional Cu-based catalysts and the state-of-the-art catalysts

Catalyst	Reaction conditions				Catalytic performance		Ref.
	P (bar), T (°C)	Space velocity	H_2/CO_2	CO_2 Conversion	Methanol selectivity	STY_{MeOH}[b] ($g_{MeOH} \cdot g_{cat}^{-1} \cdot h^{-1}$)	
1. Copre-Rh/(5In5Al)O	45, 290	(W)[a] 18000 mL g^{-1} h^{-1}	3	14.9	71.7	0.69	This work
	45, 270	(W) 18000 mL g^{-1} h^{-1}	3	9.8	84.4	0.53	
	45, 270	(W) 18000 mL g^{-1} h^{-1}	2	4.5	86.5	0.33	
	45, 270	(W) 18000 mL g^{-1} h^{-1}	1	2.6	83.1	0.28	
	45, 270	(W) 18000 mL g^{-1} h^{-1}	0.5	1.5	78.3	0.20	
	45, 270	(W) 18000 mL g^{-1} h^{-1}	0.3	1.1	73.2	0.16	
	45, 270	(W) 22500 mL g^{-1} h^{-1}	3	9.4	84.5	0.64	
	45, 270	(W) 27000 mL g^{-1} h^{-1}	3	8.2	89.6	0.71	
	45, 270	(W) 36000 mL g^{-1} h^{-1}	3	7.2	90.8	0.84	
	45, 270	(W) 45000 mL g^{-1} h^{-1}	3	6.8	91.2	1.00	
	45, 270	(W) 135000 mL g^{-1} h^{-1}	3	2.2	99.2	1.05	
	20, 290	(W) 18000 mL g^{-1} h^{-1}	3	8.1	69.2	0.36	
	1, 230	(W) 18000 mL g^{-1} h^{-1}	3	0.9	60.5	0.04	
2. CuZnGa AMO-LDH	45, 270	(W) 18000 mL g^{-1} h^{-1}	3	18.6	47.8	0.59	[1]
3. Pd@Zn	45, 270	(W) 18000 mL g^{-1} h^{-1}	3	ca. 14.4	64.9	0.60	[2]
	20, 270	(W) 18000 mL g^{-1} h^{-1}	3	ca. 7	67.3	0.30	[3]
4. PdZn/ZIF-8	45, 270	(W) 21600 mL g^{-1} h^{-1}	3	14.5	56.2	0.65	[4]
5. Pd/In$_2$O$_3$	50, 300	(W) 21000 mL g^{-1} h^{-1}	4	20	70	0.89	[5]
6. PdIn-In$_2$O$_3$/SiO$_2$	50, 300	(W) 63000 mL g^{-1} h^{-1}	4	N.A.	24	ca. 0.3[c]	[6]
7. Pd-In$_2$O$_3$ CP	50, 280	(W) 48000 mL g^{-1} h^{-1}	4	9.7	78	1.01	[7]
8. Ni$_5$Ga$_3$/SiO$_2$	1, 210	(G) 6000 h^{-1}	3	N.A.	N.A.	ca. 0.02[c]	[12]
9. In$_2$O$_3$/ZrO$_2$	50, 300	(G) 16,000 h^{-1}	4	5.2	99.8	0.30	[14]
10. ZnO-ZrO$_2$	50, 320	(W) 24000 mL g^{-1} h^{-1}	3	10	86	0.73	[15]
	20, 300	(W) 24000 mL g^{-1} h^{-1}	3	3.4	87	0.25	

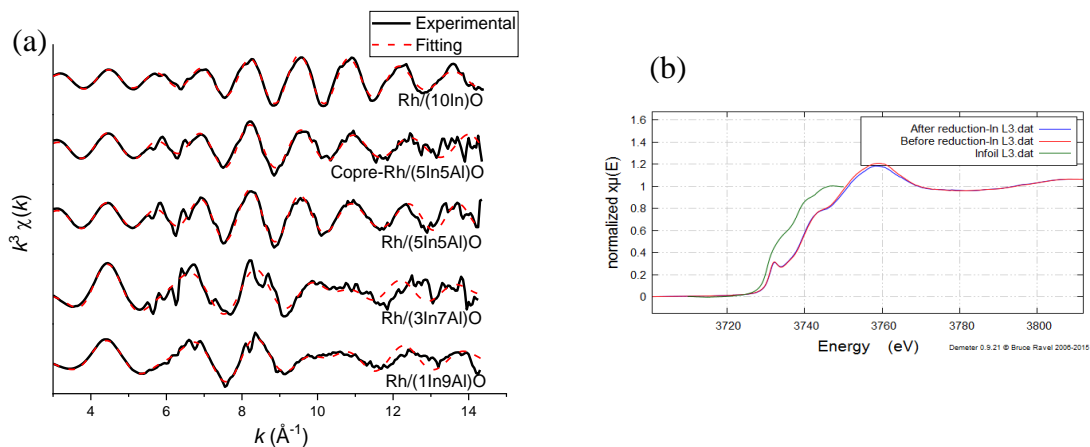[a](G) = GHSV = volume flow rate/bed volume, (W) = WHSV = mass flow rate/catalyst mass.

[b] STY: Space-time yield of methanol ($g_{MeOH} \cdot g_{cat}^{-1} \cdot h^{-1}$) calculated in this work (Copre-Rh/(5In5Al)O) as well as those reported in the references.

[c] STY estimated from the methanol production rate and the weight of the catalyst given in the reference.

5. Supplementary result of X-ray absorption spectroscopy analysis

Fig. S6 a) k^3-weighted Rh K-edge EXAFS spectra for the reduced Rh-containing catalysts. b) In L_3-edge XANES spectra of the co-RhIn/(5In5Al)O catalyst before and after H_2 reduction with In foil as the reference. As seen, most In species in co-RhIn/(5In5Al)O catalyst stay as oxidic forms both before and after H_2 reduction.

SUPPORTING INFORMATION

Table S2 The structural fitting parameters of the Rh K-edge EXAFS of the reduced Rh-containing samples.

Sample	Scatterer	R (Å)	C.N.	D-W	R factor
im-RhIn/(1In9Al)O	O	2.04(1)	3.3(1)	0.004(1)	0.5%
	Rh	2.66(1)	2.3(1)	0.008(1)	
	Rh	3.05(3)	0.8(2)	0.015(2)	
im-RhIn/(3In7Al)O	O	2.07(1)	2.9(2)	0.005(1)	1.9%
	Rh, In	2.68(1)	2.3(2)	0.011(1)	
	Rh, In	2.94(2)	1.0(2)	0.011(2)	
im-RhIn/(5In5Al)O	O	2.04(2)	0.5(1)	0.006(2)	0.6%
	In	2.64(1)	3.3(1)	0.006(1)	
	Rh	2.71(1)	2.4(2)	0.005(1)	
	In	2.82(2)	2.1(2)	0.007(2)	
	Rh	3.07(2)	1.7(4)	0.007(2)	
co-RhIn/(5In5Al)O	O	2.06(2)	0.6(2)	0.005(2)	1.4%
	In	2.62(2)	3.1(3)	0.004(2)	
	Rh	2.73(3)	1.9(2)	0.004(1)	
	In	2.83(1)	2.5(3)	0.010(2)	
	Rh	3.07(2)	2.3(4)	0.015(2)	
im-RhIn/In$_2$O$_3$	In	2.64(1)	4.4(1)	0.004(1)	0.4%
	Rh	2.73(1)	2.3(2)	0.004(1)	
	In	2.80(1)	1.4(3)	0.007(2)	
	Rh	3.03(1)	1.4(3)	0.006(2)	

6. Computational Details

The spin-polarised DFT calculations were performed using the *Vienna ab initio Simulation Package* (*VASP*).[16] The Perdew–Burke–Ernzerhof exchange-correlation functional[17] with a kinetic energy cutoff of 400 eV was used for all calculations. The project-augmented wave (PAW) method was used to describe the core–valence electron interactions.[18] We used a Hellman−Feynman force criterion of 0.02 eV/Å on each relaxed ion.

The bulk Rh and Cu were optimised using a 16 × 16 × 16 Monkhorst–Pack *k*-points grid mesh. The calculated lattice parameters of the bulk Rh and Cu are 3.82 and 3.63 Å, respectively, which are very close to the corresponding experimental values of 3.80 and 3.61 Å.

The pure Rh(111) surface was modeled using a four-layer slab repeated in a 2 × 2 surface unit cell; the pure Rh(211) and pure Cu(211) contain five layers of metal in the [111] direction and are repeated in a 2 × 4 surface unit cell; two In-doped Rh(211) with half or all Rh at the step edges substituted by In and two Zn-doped Cu(211) with half or all Cu at the step edges substituted by Zn were constructed to simulate RhIn and CuZn surface alloys (Fig. S7). For each surface slab model, only the bottom layer was fixed (to the bulk parameters) during optimization. The *k*-point mesh was sampled using a 5 × 5 × 1 Monkhorst-Pack grid. To avoid interactions between slabs, all slabs were separated by a vacuum gap greater than 14 Å.

The H adsorption energy (E_{ads}) was calculated by:

$$E_{ads} = E_{H/sub} - E_{sub} - \tfrac{1}{2}E_{H2},$$

where $E_{H/sub}$, E_{sub}, and E_{H2} are the DFT energies of the adsorption complex, clean substrate, and gas-phase H_2 molecule, respectively.

The energies of adsorbed HCOO and COOH species (denoted as E_{HCOO^*} and E_{COOH^*}) were calculated respectively by:

$$E_{HCOO^*} = E_{HCOO/sub} - E_{sub},$$
$$E_{COOH^*} = E_{COOH/sub} - E_{sub},$$

where $E_{HCOO/sub}$, $E_{COOH/sub}$, and E_{sub} are the DFT energies of the HCOO/substrate adsorption complex, COOH/substrate adsorption complex, and clean substrate, respectively.
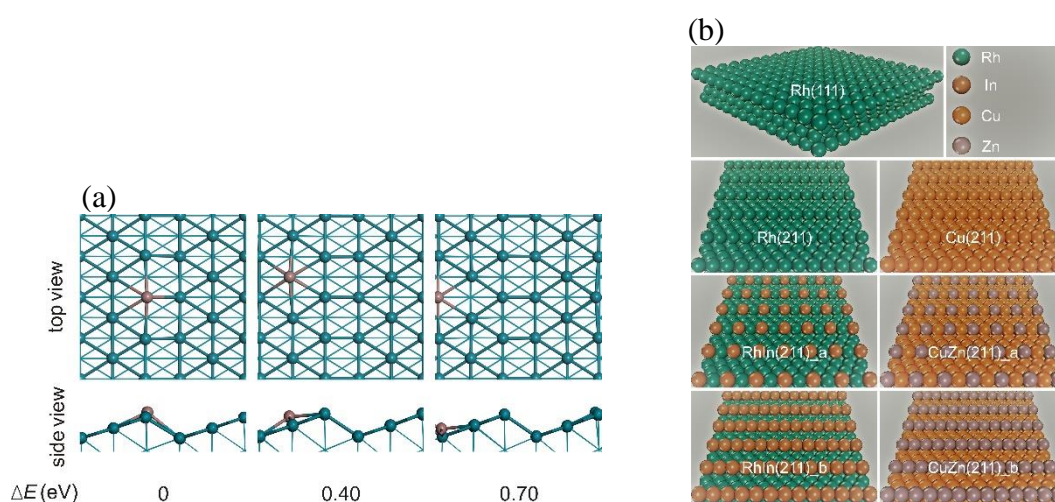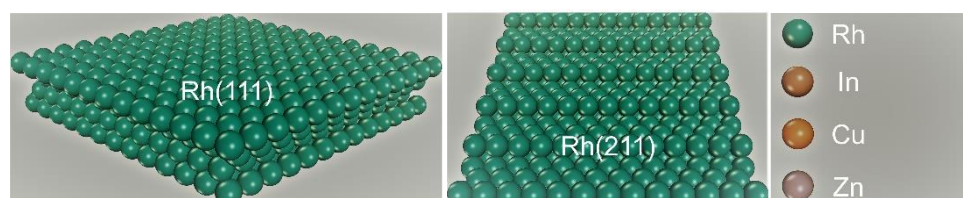
The selection of the Rh surface model

The flat Rh(111) and the stepped Rh(211) surfaces were first determined to represent the Rh catalysts without and with surface defects, respectively. Table S3 shows calculated H adsorption energies (E_{ads}, in eV) and energies of adsorbed HCOO and COOH species (E_{HCOO^*} and E_{COOH^*}, in eV) on Rh(111) and Rh(211). As can be seen that Rh(211) with step edges has stronger H, HCOO, and COOH binding energies than the ideal defect-free Rh(111), indicating the effect of surface defects. To study the effect of indium doping, we then constructed RhIn surface alloys. Considering the small size (more surface defects) of the synthesised In-modified Rh catalyst nanoparticles (the majority is 1-3 nm), the (211) surface should be a more realistic model than the (111) surface for the further study of the indium doping effect.

Table S3. Calculated H adsorption energies (E_{ads}, in eV) and energies of adsorbed HCOO and COOH species (E_{HCOO^*} and E_{COOH^*}, in eV) on Rh(111) and Rh(211).

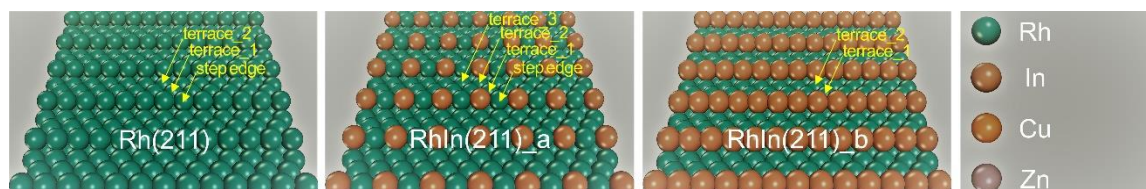|	E_{ads}	E_{HCOO^*}	E_{COOH^*}	E_{diff}
Rh(111)	-0.55	-27.02	-27.01	-0.01
Rh(211)	-0.59	-27.62	-27.37	-0.25

Fig. S7 a) Optimised structures and relative energies of single-In-doped Rh(211). Rh and In atoms are in cyan and brown, respectively. Only the first layer of metals is represented by balls; the other layers of metals are represented by lines. The result indicates that In strongly favours to substitute Rh at the step edge site. b) Perspective views of Rh(111), Rh(211), RhIn(211)_a, RhIn(211)_b, Cu(211), CuZn(211)_a, and CuZn(211)_b. The pure Rh(111) surface was modeled using a four-layer slab repeated in a 2 × 2 surface unit cell; the pure Rh(211) and pure Cu(211) contain five layers in the [111] direction and are repeated in a 2 × 4 surface unit cell; two In-doped Rh(211) (RhIn(211)_a and RhIn(211)_b, respectively) with 50% or 100% of the step-edge Rh sites substituted by In, and two Zn-doped Cu(211) (CuZn(211)_a and CuZn(211)_b, respectively) with 50% or 100% step-edge Cu sites substituted by Zn were constructed to simulate RhIn and CuZn surface alloys.

Table S4. Bader charges of surface Rh and indium-modified Rh.

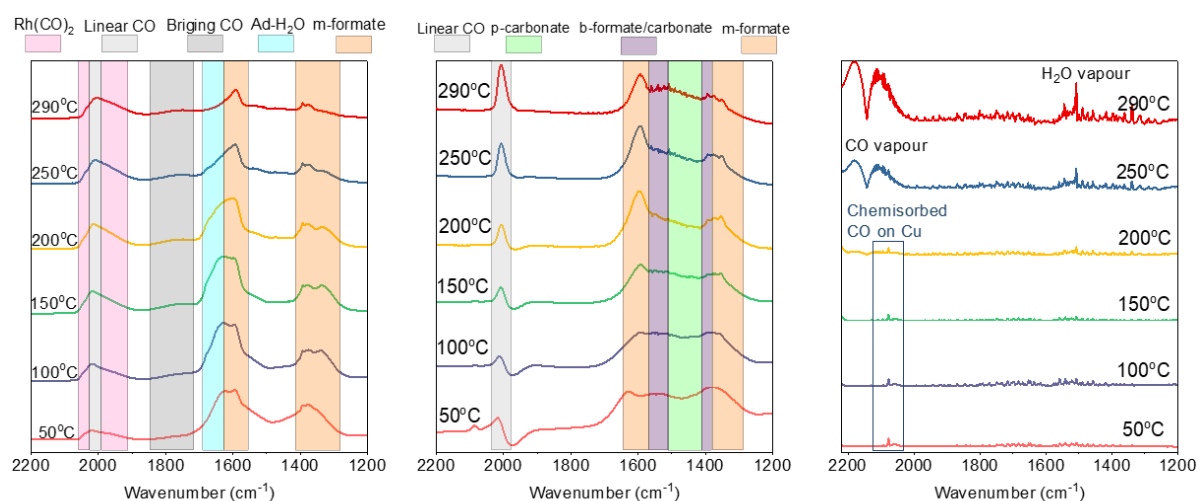|	Rh(211)	RhIn(211)_a	RhIn(211)_b
step edge	-0.06	-1.60	/
terrace_1	-0.01	-0.30	-0.74
terrace_2	-0.03	-0.47	-0.55
terrace_3	/	-0.02	/

7. Supplementary result of in-situ FTIR analysis

Fig. S8 shows that in the co-Rh/Al$_2$O$_3$ sample (no In addition), the Rh(CO)$_2$ gem-dicarbonyls species (through Rh-C interaction) were adsorbed on Rh, giving the peaks at 1960-1990 cm^{-1} and 2030-2050 cm^{-1}.[19] Other weakly adsorbed species, namely linear CO, bridging CO, adsorbed H$_2$O, and mono-dentate formate[20,21] could also be observed in the temperature range from 50 °C to 290 °C, but the intensities of the adsorbed H$_2$O and mono-dentate formate greatly decreased as temperature increased. In contrast, the co-RhIn/(5In5Al)O sample showed different adsorbed species on the surface where the intermediates including bi-dentate and poly-dentate carbonates as well as mono-dentate and bi-dentate formates (formed via adsorbed HCOO), which are regarded as the key intermediates for the methanol production,[22,23] were prevalently observed. It can also be noted that a weak band attributed to the linear CO appeared at around 2000-2010 cm^{-1}.[24] As the temperature was raised, this linear CO band was apparently increased. However, there was no formation of characteristic strong and broad bands of 2110 and 2180 cm^{-1} attributable to the gas-phase CO.[25] Thus, this surface CO (and COOH) is expected to be in equilibrium with other surface species (i.e. HCOO) without the direct desorption to the gaseous CO. As for the Cu/ZnO/Al$_2$O$_3$ catalyst, the small sharp peaks at around 2060-2080 cm^{-1} are the bands corresponding to the chemisorbed CO on a low Miller-index plane of Cu.[23] As the temperature increased, the vibrations of water vapour enhanced. In addition, two strong and broad bands at 2110 and 2180 cm^{-1} attributed to the gas-phase CO demonstrated that the RWGS reaction is favoured on this catalyst.[25] Note that the absence of the surface adsorbed intermediates on Cu/ZnO/Al$_2$O$_3$ catalyst is showing a consequence of the low residence time as well as relatively weak adsorption on the Cu-based surface

Fig. S8. In-situ FTIR spectra of the adsorbed species on the reduced catalysts. A gas flow of 25% CO$_2$ and 75% H$_2$ is passed through the catalyst pellets made by 20 mg of samples at various temperatures.

8. A discussion on the active sites in the co-RhIn/(5In5Al)O catalyst

It is clear from our characterisations that Rh-In_2O_3 metal-support interaction could lead to electronic modification of Rh and the EXAFS data of Rh-In can account for such interaction. Although this direct interaction could be taken place, the readily hydrogen spillover from Rh can concomitantly lead to the reduction of In_2O_3 to give $RhIn_x$ species (Rh on In_2O_3 is clearly unstable under the conditions). From the XPS result, we noted that the partial reduction of In_2O_3 was clearly taken place to give In^0 when this supported catalyst was subjected to H_2 exposure. Besides, dark clusters in the TEM images of both reduced and spent co-RhIn/(5In5Al)O were found to have Rh-In alloy structures. Therefore, Rh-In bimetallic species are the result of the identified solid products to be responsible for the enhanced methanol selectivity. Since we cannot exclude the possibility that the 4d-orbitals of indium ion (post-transition metal ion) although being contracted to the core may still directly overlap with that of metallic Rh to offer an electronic modification, we propose to investigate the use of In ions in a totally stable solid matrix to verify the direct metal-support interaction in future.

SUPPORTING INFORMATION

References

[1] M. M.-J. Li, C. Chen, T. Ayvali, H. Suo, J. Zheng, I. Teixeira, L. Ye, H. Zou, D. O'Hare, S. C. E. Tsang, *ACS Catal.* **2018**, *8*, 4390–4401.

[2] F. Liao, X.-P. Wu, J. Zheng, M.-J. Li, Z. Zeng, X. Hong, A. Kroner, Y. Yuan, X.-Q. Gong, S. C. E. Tsang, *Catal. Sci. Technol.* **2016**, *6*, 7698–7702.

[3] F. Liao, X.-P. Wu, J. Zheng, M. M.-J. Li, A. Kroner, Z. Zeng, X. Hong, Y. Yuan, X.-Q. Gong, S. C. E. Tsang, *Green Chem.* **2017**, *19*, 270–280.

[4] Y. Yin, B. Hu, X. Li, X. Zhou, X. Hong, G. Liu, *Appl. Catal. B Environ.* **2018**, *234*, 143–152.

[5] N. Rui, Z. Wang, K. Sun, J. Ye, Q. Ge, C. Liu, *Appl. Catal. B, Environ.* **2017**, *218*, 488–497.

[6] J. L. Snider, V. Streibel, M. A. Hubert, T. S. Choksi, E. Valle, D. C. Upham, J. Schumann, M. S. Duyar, A. Gallo, F. Abild-Pedersen, et al., *ACS Catal.* **2019**, *9*, 3399–3412.

[7] M. S. Frei, C. Mondelli, R. García-Muelas, K. S. Kley, B. Puértolas, N. López, O. V. Safonova, J. A. Stewart, D. Curulla Ferré, J. Pérez-Ramírez, *Nat. Commun.* **2019**, *10*, 3377.

[8] J. Graciani, K. Mudiyanselage, F. Xu, A. E. Baber, J. Evans, S. D. Senanayake, D. J. Stacchiola, P. Liu, J. Hrbek, J. Fernández Sanz, et al., *Science* **2014**, *345*, 546–50.

[9] L. Lin, S. Yao, Z. Liu, F. Zhang, N. Li, D. Vovchok, A. Martínez-Arias, R. Castañeda, J. Lin, S. D. Senanayake, et al., *J. Phys. Chem. C* **2018**, *122*, 12934–12943.

[10] S. Yang, S. H. Pang, T. P. Sulmonetti, W. Su, J. Lee, B. Hwang, C. W. Jones, *ACS Catal.* **2018**, *8*, 12056–12066.

[11] B. Ouyang, W. Tan, B. Liu, *Catal. Commun.* **2017**, *95*, 36–39.

[12] F. Studt, I. Sharafutdinov, F. Abild-Pedersen, C. F. Elkjær, J. S. Hummelshøj, S. Dahl, I. Chorkendorff, J. K. Nørskov, *Nat. Chem.* **2014**, *6*, 320–324.

[13] E. M. Fiordaliso, I. Sharafutdinov, H. W. P. Carvalho, J. D. Grunwaldt, T. W. Hansen, I. Chorkendorff, J. B. Wagner, C. D. Damsgaard, *ACS Catal.* **2015**, *5*, 5827–5836.

[14] O. Martin, A. J. Martín, C. Mondelli, S. Mitchell, T. F. Segawa, R. Hauert, C. Drouilly, D. Curulla-Ferré, J. Pérez-Ramírez, *Angew. Chemie Int. Ed.* **2016**, *55*, 6261–6265.

[15] J. Wang, G. Li, Z. Li, C. Tang, Z. Feng, H. An, H. Liu, T. Liu, C. Li, *Sci. Adv.* **2017**, *3*, e1701290.

[16] G. Kresse, J. Hafner, *Phys. Rev. B* **1994**, *49*, 14251–14269.

[17] J. P. Perdew, K. Burke, M. Ernzerhof, *Phys. Rev. Lett.* **1996**, *77*, 3865–3868.

[18] P. E. Blöchl, *Phys. Rev. B* **1994**, *50*, 17953–17979.

[19] A. Beuls, C. Swalus, M. Jacquemin, G. Heyen, A. Karelovic, P. Ruiz, *Appl. Catal. B Environ.* **2012**, *113–114*, 2–10.

[20] A. Karelovic, P. Ruiz, *ACS Catal.* **2013**, *3*, 2799–2812.

[21] A. Karelovic, P. Ruiz, *Appl. Catal. B Environ.* **2012**, *113–114*, 237–249.

[22] S. Collins, M. Baltanas, A. Bonivardi, *J. Catal.* **2004**, *226*, 410–421.

[23] Q. Sun, C.-W. Liu, W. Pan, Q.-M. Zhu, J.-F. Deng, *Appl. Catal. A Gen.* **1998**, *171*, 301–308.

[24] F. Solymosi, A. Erdöhelyi, T. Bánsági, *J. Chem. Soc. Faraday Trans. 1* **1981**, *77*, 2645.

[25] G. J. Millar, C. H. Rochester, K. C. Waugh, *Catal. Letters* **1992**, *14*, 289–295.